Ultrasound in Medicine & Biology 51 (2025) 1831–1839

Contents lists available at ScienceDirect

Ultrasound in Medicine & Biology

journal homepage: www.elsevier.com/locate/ultrasmedbio

Original Contribution

Pulse-Echo Imaging of Breast Speed of Sound as a Potential Biomarker for Breast Cancer

Dieter Schweizer [a,*], Monika Farkas [b], Can Deniz Bezek [d], Anna Potempa [b], Cornelia Leo [c], Rahel A. Kubik-Huch [b,c], Orcun Goksel [a,d]

[a] Computer-assisted Applications in Medicine Group, ETH Zurich, Zurich, Switzerland
[b] Department of Radiology, Kantonsspital Baden, Baden, Switzerland
[c] Breast Center, Kantonsspital Baden, Baden, Switzerland
[d] Department of Information Technology, Uppsala University, Uppsala, Sweden

ARTICLE INFO

Keywords:
Breast cancer
Speed-of-sound imaging
Malignancy classification

ABSTRACT

Objective: Speed-of-sound (SoS) images, derived from minute misalignments between ultrasound images consecutively acquired using a motion-robust technique, were studied with multi-frame acquisitions to derive a lesion assessment metric for the differential diagnosis of breast cancer.
Methods: SoS elevation within inclusions was characterized as SoS contrast by comparing inclusions with their surrounding tissue. Malignancy was predicted as having larger SoS contrast compared with benign inclusions. In a study involving 100 patients with various breast lesion types, the findings were compared with gold standard diagnoses based on biopsy and expert consensus.
Results: The proposed SoS contrast metric achieved an overall malignancy classification with an area under the curve of 69.70% (95% confidence interval [CI]: 57.4%–81.2%), with results varying depending on lesion type. Accounting for breast density or lesion size improved the area under the curve to 77.40% (95% CI: 59.2%–93.3%) and 78.09% (95% CI: 56.2%–95.8%), respectively. Focusing on Breast Imaging Reporting and Data System 4 lesions, where mammography and B-mode imaging are inconclusive, a sensitivity of 25% at 100% specificity or a specificity of 23% at 100% sensitivity was attained.
Conclusion: This study highlights the feasibility of SoS contrast as an imaging biomarker for the differential diagnosis of breast lesions. It also indicates the need for further technical advancements in SoS imaging to strengthen its ability to effectively classify lesions and enable interactive measurements during ultrasound examinations.

Introduction

Patients with a palpable lump in the breast or suspicious findings on X-ray mammography typically undergo breast ultrasound (BUS) examination as a supplemental imaging modality. The findings are used for tumor classification using the American College of Radiology (ACR) Breast Imaging Reporting and Data System (BI-RADS) lexicon, in a scale ranging from 1 to 6 [1]. Suspicious findings are further assessed with ultrasound (US)-guided biopsy, a procedure that causes patient discomfort, emotional stress and may involve a risk of complications such as bleeding, infection or tumor seeding. Conventional BUS B-mode imaging lacks the specificity needed to reliably differentiate malignant from benign tissues in all cases. According to the ACR BI-RADS lexicon [1], lesions with a risk of malignancy between 2% and 95% are classified as BI-RADS 4, requiring biopsy for pathological assessment unless the patient declines. BI-RADS 3 lesions, with a risk of malignancy below 2%, are typically managed with watchful waiting and close follow-up, although a biopsy may be performed at the patient's request. Novel imaging biomarkers could provide additional diagnostic information to improve lesion classification accuracy during BUS and to stratify cases requiring biopsy. Such biomarkers could eventually be integrated into tumor classification guidelines, similar to recently established biomarkers such as shear wave elastography, which evaluates tissue Young's modulus and has been included in clinical guidelines [2]. Comparatively, in the study by Glozman and Azhari [3] it was shown that shear wave speed may vary substantially for a given tissue, *e.g.*, based on how it is measured, precompression, *etc.*, while bulk modulus-based speed of sound (SoS) is a more repeatable metric. In this paper, we study SoS as one such novel imaging modality that enables quantitative measurements and, therefore, objective assessment. This may in the

* Corresponding author at: ETH Zurich, D-ITET, CVLab, Sternwartstrasse 7, 8092 Zurich, Switzerland.
E-mail address: dieter.schweizer@vision.ee.ethz.ch (D. Schweizer).
Dieter Schweizer and Monika Farkas contributed equally to this manuscript; Rahel A. Kubik-Huch and Orcun Goksel act as shared last author.
Kantonspital Baden is an affiliated Hospital for Research and Teaching of the Faculty of Medicine of the University of Zurich.

https://doi.org/10.1016/j.ultrasmedbio.2025.07.002
Received 20 December 2024; Revised 24 June 2025; Accepted 1 July 2025

0301-5629/© 2025 The Author(s). Published by Elsevier Inc. on behalf of World Federation for Ultrasound in Medicine & Biology. This is an open access article under the CC BY license (http://creativecommons.org/licenses/by/4.0/)

future act as a complementary imaging modality for classifying breast lesions.

Previous studies have demonstrated a correlation between increased SoS and attenuation of US waves in cancerous tissues [4,5]. Several methods [6–12] have been proposed to measure such tissue properties using transmission (Tx)-based US techniques or external mechanical reflectors. However, these methods require custom, complex, bulky and often costly hardware, or need tissue access from two sides, limiting their adoption in clinical settings and existing BUS workflows. In contrast, pulse-echo SoS imaging requires no custom hardware and can be performed using standard US systems and transducers, which are operated using specialized acquisition sequences and post-processing algorithms. Fourier domain [13] and spatial domain [14,15] reconstruction methods based on plane-wave Txs, as well as diverging waves [16], have been proposed to find local SoS distribution. Parabola fitting [17,18], coherence [19], compounding [20] and refraction-based [21] methods have also been utilized for SoS reconstruction. Wang et al. [22] provide an overview of pulse-echo SoS approaches.

We utilized a method where SoS maps are generated by analyzing speckle shifts within a tissue region of interest observed from two or more imaging directions using distinct US Tx sequences. SoS heterogeneity along the US beam paths causes speckle misalignment between these observations from different directions. By identifying such misalignments and encoding the related imaging physics in an algebraic form, image-reconstruction algorithms can then estimate the spatial SoS distribution. This was shown as a promising biomarker for characterizing breast lesions in a pilot study with 20 patients [23]. To reduce artifacts from intrinsic or operator-induced motion between multiple Tx acquisitions, a specialized sequence with virtual source (VS) Tx was proposed for *in vivo* SoS imaging [24].

The objective of this study was to apply the improved motion-robust SoS imaging technique on a significant number of patients to quantitatively image various types of breast lesions with a multi-frame acquisition for robustness, develop a refined technique and metric for lesion assessment, and evaluate its effectiveness in distinguishing between benign and malignant lesions. Breast imaging with SoS applied together with B-mode is referred to here as multi-parametric breast ultrasound (mpBUS).

Materials and methods

A prospective study approved by the ethics committee (EKNZ, Switzerland, NCT04480437), was conducted at Kantonsspital Baden (Switzerland) under external monitoring and with the informed consent of the participants. US data collected from breast lesions was retrospectively analyzed to reconstruct spatial SoS maps, which served to classify the lesions as benign or malignant. The results were compared against standard clinical findings that were determined based on biopsy or expert consensus. To ensure confidentiality, all data and findings were collected as encoded, preventing direct identification of participants.

Study population

Patients aged 18 years or older who underwent diagnostic examinations for potential breast lesions, based on prior findings from mammography, magnetic resonance imaging or BUS, or due to palpable abnormalities, were invited to participate in the study. Patients who were breastfeeding, experiencing mastitis or classified as vulnerable were excluded.

A total of 100 participants were enrolled and divided into two groups of 50 each: Group 1 comprised patients scheduled for US-guided core needle biopsy, including those with suspicious lesions classified as BI-RADS 4 for pathological assessment, lesions requiring further characterization in classes 5 and 6, and selected cases of BI-RADS 3 (*e.g.*, given a valid request by the patient); Group 2 consisted of patients not undergoing biopsy, *i.e.*, those with a BI-RADS classification 2 or 3, where diagnoses were determined by expert consensus based on patient history, existing imaging and laboratory test results. The distribution of the study population by BI-RADS class is summarized in Table 1. Additional metadata, such as age, hormonal status and ACR breast density [1], are also provided in this table. Given that some patients had multiple lesions, a total of 124 lesions were assessed using BUS. Based on the final diagnoses, these lesions were broadly categorized as follows: malignant lesions, including ductal carcinomas; benign lesions, further classified as simple cysts (fluid-only), complex cysts (fluid and tissue) and fibroadenomas; and others atypical benign lesions. The distribution of the lesion findings between the groups of patients is given in Table 2. Additionally, lesion dimensions measured during BUS are summarized in Table 3. Sizes are reported with respect to the US imaging view, with size-L for the lateral (horizontal), size-A for the axial (vertical) and size-E for the elevational (out-of-plane) dimension.

Data collection

Standard BUS imaging was performed using a Logic E10 ultrasound system (GE Healthcare, Chicago, IL, USA). Up to three lesions were localized, and reference images were taken with annotations of size and distance from the mamilla (recorded to help attribute biopsy results to different lesions where applicable).

As the reference (GE Healthcare) system could not output raw radiofrequency (RF) data, which are required to reconstruct SoS maps, we used an additional US machine as our mpBUS system. RF data were acquired from the same lesion locations for four to seven different views using a UF-760AG ultrasound system (Fukuda Denshi, Tokyo, Japan) with a FUT-LA385-12P linear array transducer (128 elements, 300 μm

Table 1
Study population.

Classification	Class	Group 1	Group 2	Total
Age (years), mean (range)		56.16 (23-85)	51.46 (23–82)	53.81 (23–85)
BI-RADS class	2	0	29	29
	3	2	21	23
	4	25	0	25
	5	22	0	22
	6	1	0	1
ACR breast density	A	2	0	2
	B	19	12	31
	C	24	23	47
	D	2	10	12
	Not known	3	5	8
Hormonal status	pre-menopausal	11	19	30
	Post-menopausal	30	22	52
	Not known	9	9	18
	Hormone replacement	7	7	14

Table 2
Lesion findings given gold standard diagnoses (biopsy for group 1 and expert consensus for group 2).

Type	Sub-type	Group 1	Group 2	Total
Benign	Simple cyst	0	14	14
	Complex cyst	0	11	11
	Fibroadenoma	14	30	44
Malignant	Invasive ductal carcinoma	27	0	27
	Invasive lobular carcinoma, classic sub-type	2	0	2
	Invasive lobular carcinoma, pleomorphic sub-type	4	0	4
Other	Mastopathic changes	0	4	4
	Sclerosing adenosis	1	2	3
	Scar	0	3	3
	Hamartoma	0	2	2
	Fibrocystic changes and papilloma	1	0	1
	Papilloma	1	1	2
	Atypical ductal hyperplasia	1	0	1
	Fat with nodular fibrosis	1	0	1
	Breast parenchyma with nodular fibrosis	1	0	1
	Normal breast parenchyma	1	0	1
	Cystic wall	1	0	1
	Fibrocystic changes with pseudoangiomatous stromal hyperplasia	1	0	1
	Cystic conglomerate	0	1	1

pitch, 7.5 MHz center frequency, 69% bandwidth and 40.96 MHz RF sampling frequency). Two successive acquisitions were captured per view. During acquisition, data were temporarily stored in transducer element buffers until the echo signal from the deepest imaged location was received. Received data were then transported in groups of elements over a high-speed data link to an attached PC for storage and processing, before initiating the next transmit–receive cycle. Keeping the reference system (GE Healthcare) together with the mpBUS system (Fukuda Denshi) allowed us to conform to the standard clinical workflow for BUS diagnostics or BUS biopsy.

For group 1 patients, US-guided core needle biopsies were performed using 14-gauge needles with the reference US system. Diagnoses for group 1 patients were then based on the histopathological examination of these biopsy samples. Diagnoses for group 2 patients were determined based on reference US images by expert consensus from two radiologists specializing in female breast imaging, with a third expert included in cases of disagreement.

The ACR breast density classification was determined by expert consensus based on mammography images conducted prior to the BUS exam. ACR density classification was not available for eight patients who were excluded from mammography either due to their young age or previous recommendations. Note that BUS imaging was nevertheless performed for these eight patients.

Data processing and SoS-based inclusion classification

SoS reconstruction was performed as described by Schweizer et al. [24] and briefly summarized here as follows: We used a VS sequence with 17 Txs equally distributed over the transducer surface. With a transmit f-number of 1.0, 31 elements transmitted each diverging wave. Each RF raw data set received by all 128 receive channels was recorded for retrospective processing. From every two consecutive RF frames, the speckle misalignment was determined using a displacement tracking method. Local displacement observations that were above a correlation threshold ensuring sufficient quality were then utilized by an SoS reconstruction model, which also includes spatial regularization (kept constant for all reconstructions in this study). This process yielded a spatial map of SoS distribution in the tissue, based on which we assessed the imaged lesions. As such distributions may depend on the initial beamforming SoS assumption, to account for variations across the population we repeated the above process three times for each mpBUS acquisition, each time updating the beamforming SoS as the average of the preceding SoS distribution. The SoS map from the third iteration is used for cancer assessment herein. The lesions were annotated by a radiologist on B-mode images that were acquired during the mpBUS SoS data acquisition with the Fukuda Denshi US system, hence the annotations being representative of the SoS reconstructions. We assessed the tumor contrast with its background, which was defined as areas outside the inclusion, with an added margin of 5 mm to minimize inaccuracies that may arise from delineation and reconstruction processes.

Contrast was calculated as $\Delta\mathrm{SoS} = \mu_{\mathrm{inc}} - \mu_{\mathrm{bkg}}$,where μ_{inc} represents the 95%-ile of SoS within the inclusion and μ_{bkg} denotes the median SoS of the background. Using the 95%-ile aims to capture the highest SoS inclusion values while maintaining robustness against potential superfluous pixel-wise variations. This intends to account for tumor heterogeneity [25] for assessing inclusions based on their highest SoS tissue sub-region (that covers more than 5% of annotated inclusion cross-sections).

For robustness to potential variation across individual acquisitions, such as errors due to in-plane motion and morphological differences due to tumor heterogeneity, we leveraged information from multiple lesion views by defining lesion contrast as the median of the individual SoS contrast values derived from different views. Figure 1 illustrates the SoS contrast calculation in a carcinoma example. Based on this SoS contrast, lesions exceeding a specified threshold were classified as malignant, while those below the threshold were classified as benign.

Table 3
Lesion size [mm] for the lateral (horizontal), axial (vertical) and elevational dimensions with respect to the ultrasound view.

Type	Sub-type	Size-L	Size-A	Size-E
Benign	Simple cyst complex cyst	3.5–52.4	1.7–25.2	3.6–52.6
	fibroadenoma	2.1–11.0	1.4–11.2	2.4–14.1
		3.7–29.6	2.3–20.9	3.7–32.8
Malignant	Carcinoma	3.1–26.8	2.9–27.2	1.7–37.9
Other	As in Table 2	3.9–28.0	2.0–19.5	3.5–35.8

Statistical analysis

Statistical analysis was conducted using MATLAB (2022b, The MathWorks Inc, Natick, MA, USA) software. Studied sub-group sizes for benign (N_b) and malignant (N_m) samples are reported in the figures, as well as indicating their SoS contrast mean and standard deviation (mean ± std). The null hypothesis of sub-group SoS contrast similarity was assessed using the unpaired Student's *t*-test, with statistical significances indicated with *** for $p \leq 0.001$, ** for $0.001 < p \leq 0.01$, * for $0.01 < p < 0.05$ and "ns" for no statistical significance for higher *p*-values. For the reported values from the receiver operator characteristic (ROC) analyses, we also indicated 95% confidence intervals (CIs) based on 1000-fold bootstrapping.

The above SoS-based classification, *i.e.*, malignant (SoS-based positive) and benign (SoS-based negative), for each lesion ($N = 124$), was compared with the gold standard diagnoses to categorize each finding, determining accordingly the number of true positives (*tp*), true negatives (*tn*), false positives (*fp*) or false negatives (*fn*). Based on these, the following standard metrics were calculated: Sensitivity (true-positive rate) as $tp/(tp+fn)$; specificity as $tn/(tn+fp)$; false-positive rate as $fp/(tn+fp)$, positive-predictive value (PPV) as $tp/(tp+fp)$; negative-predictive value (NPV) as $tn/(tn+fn)$; and accuracy as $(tp+tn)/N$. To assess the predictive performance of SoS contrast for malignancy, ROC curves were generated by varying the SoS threshold, with the area under the curve (AUC) serving as the primary metric. Based on ROC analysis, we also reported SoS contrast thresholds to differentiate malignant from benign lesions.

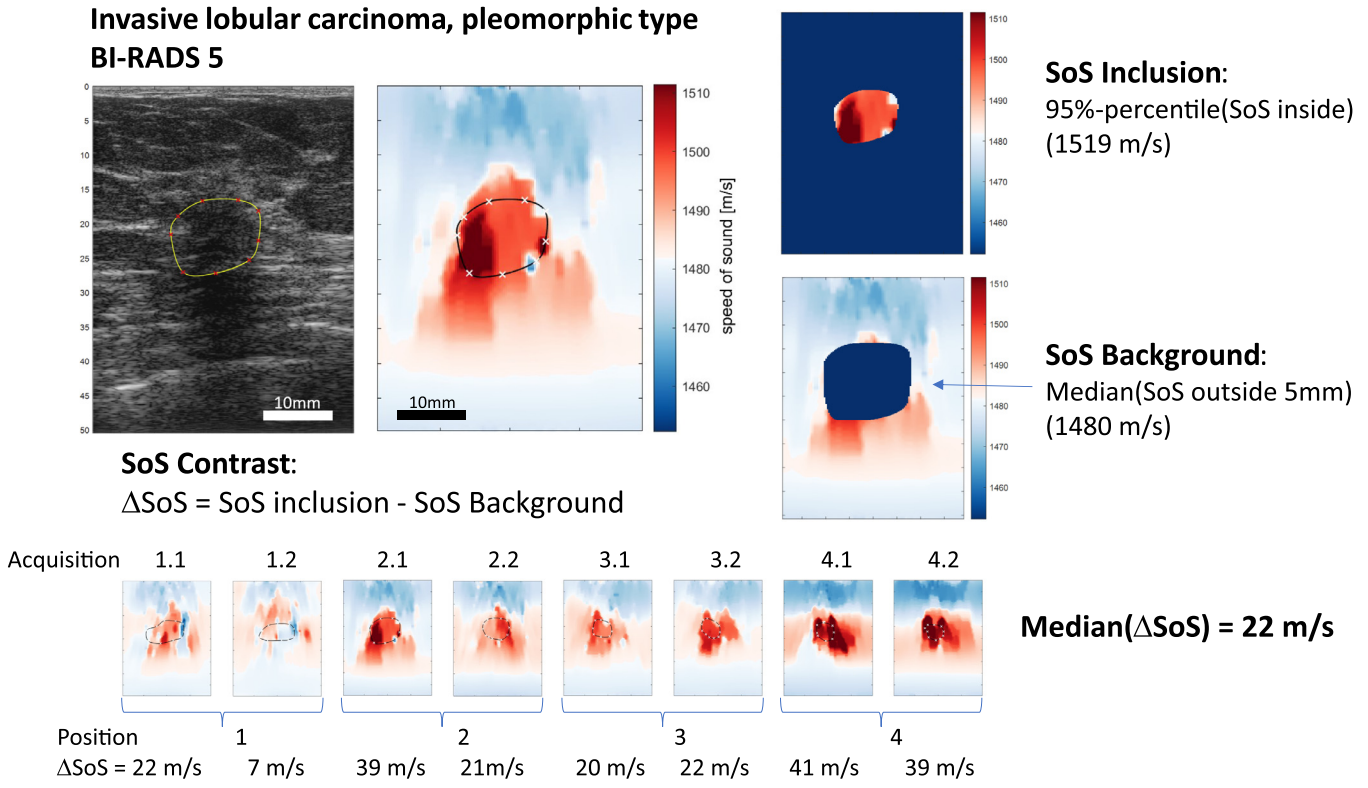

Figure 1. Illustration of speed-of-sound (SoS) contrast calculation for lesion classification. (*Top left*) B-mode and SoS views with lesion delineation. (*Top right*) SoS values masked within the inclusion and the background. (*Bottom*) Individual contrast values for eight views (four positions, each with two consecutive acquisitions), with the median contrast value used as the overall lesion SoS contrast for further analysis.

The analysis was performed on the entire set of lesions as well as on specific subsets, with comparisons including simple cysts, complex cysts and fibroadenomas individually or as a group compared with carcinoma.

Results

SoS images and contrast

Figure 2 presents sample SoS images of malignant and benign lesions, along with B-mode images from the reference BUS exam and those acquired during SoS imaging.

The median SoS contrast values, along with their inter-quartile ranges, were as follows: simple cysts 12.7 ± 4.3 m/s, complex cysts 11.2 ± 2.7 m/s, fibroadenomas 10.9 ± 3.1 m/s and invasive carcinomas 16.9 ± 6.4 m/s.

Prediction of malignancy through SoS contrast

Figure 3 presents the box plots and ROC analysis results for distinguishing malignant ($N_m = 33$, 17.9 ± 8.3 m/s) from benign ($N_b = 55$, 11.9 ± 6.4 m/s) lesions ($p = 0.0020$). In our analyses to assess the added diagnostic value of SoS, we excluded simple cysts as they are readily distinguishable from invasive carcinoma using B-mode imaging alone, making SoS or other imaging unnecessary for differential diagnosis. The SoS contrast demonstrated a predictive ability for malignancy with an AUC of 69.70% (CI: 57.4%–81.2%). Using a threshold of 18.5 m/s, the diagnostic performance achieved an accuracy of 76.14% (CI: 67.0%–85.2%), with a specificity of 89.09% (CI: 80.0%–96.4%) and a sensitivity of 54.55% (CI: 38.3%–71.7%), with a PPV of 75.00% (CI: 56.5%–91.7%) and an NPV of 76.56% (CI: 65.9%–86.4%).

Dependency of SoS contrast on breast density

The influence of breast density on the predictive ability for malignancy has also been analyzed.

Figure 4 illustrates the box plots and ROC analysis results for malignancy prediction as stratified for patients with non-dense breasts (ACR density categories A and B, $N_b = 14$, $N_m = 21$, $p = 0.2021$) and for patients with dense breasts (ACR categories C and D, $N_b = 33$, $N_m = 12$, $p = 0.0004$). For the latter group with dense breasts, the AUC resulted in 77.40% (95% CI: 59.2%–93.3%) and a SoS contrast threshold of 13.75 m/s yielded an accuracy of 82.22% (95% CI: 71.1%–93.3%), with 87.88% (95% CI: 75.9%–97.2%) specificity and 66.67% (95% CI: 36.4%–91.7%) sensitivity. As demonstrated by Bezek et al. [26], breast density can be accurately determined by global SoS measurements based on pulse-echo US acquisition and speckle shift-based processing, which can enable density-dependent stratification of cancer patients for SoS contrast-based malignancy classification during the very same exam and data acquisition.

Dependency of SoS contrast on lesion size

A second sub-analysis examined the influence of lesion size on SoS contrast, with the results presented in Figure 5. Axial lesion size (size-A) was used as the criterion for stratification, as lesions are typically smaller in this dimension compared with the other two dimensions. The median axial size of all lesions was 5.9 mm, which was used as the threshold to stratify the lesions as small ($N_b = 34$, $N_m = 10$, $p = 0.0002$) for size-A ≤5.9 mm and as large ($N_b = 21$, $N_m = 23$, $p = 0.0738$) for size-A >5.9 mm.

For small lesions, shown in Figure 5 (left column), the AUC resulted in 78.09% (95% CI: 56.2%–95.8%) and a SoS contrast threshold of 19.00 m/s achieved an accuracy of 86.36% (95% CI: 50.0%–79.5%), with 91.18% (95% CI: 81.6%–100%) specificity and 70.00% (95% CI:

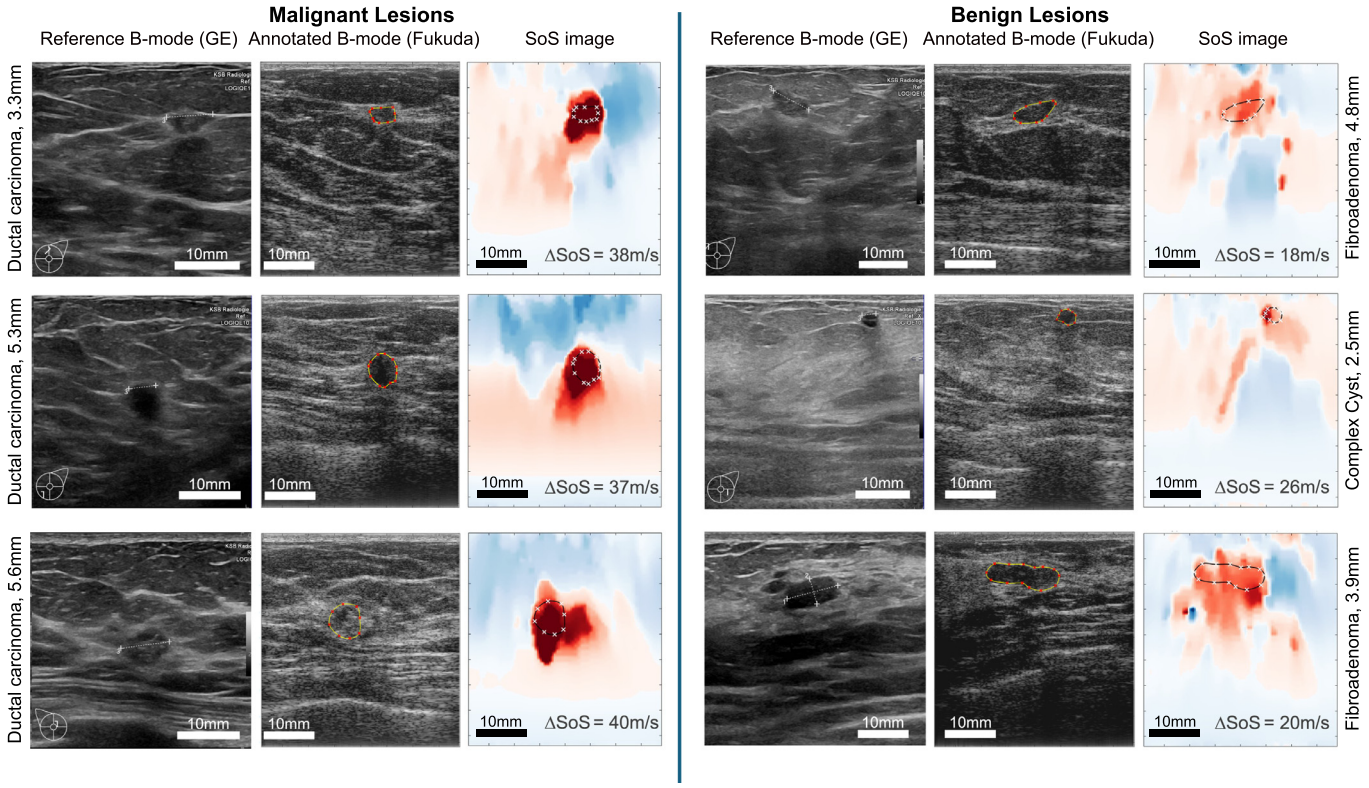

Figure 2. Examples of reconstructed speed-of-sound (SoS) images for malignant (*left*) and benign (*right*) lesions. Shown alongside are corresponding B-mode images from the reference breast ultrasound system and annotated B-mode images from the SoS acquisition system. Note that the reference and multi-parametric breast ultrasound images may show different lesion cross-sections and even flipped views (as in *top right*). Lesion size (size-A) measured in the reference image is indicated on the side.

33.3%–93.1%) sensitivity. For large lesions, shown in Figure 5 (right column), the AUC resulted in 62.94% (95% CI: 43.6%–78.9%) and a threshold of 14.75 m/s yielded an accuracy of 65.91% (95% CI: 50.0% –79.5%), with 76.19% (95% CI: 56.2%–93.3%) specificity and 56.52% (95% CI: 33.3%–75.0%) sensitivity.

Prediction of malignancy for BI-RADS 4 lesions

A third sub-analysis, as shown in Figure 6, evaluated BI-RADS 4 lesions, with the biopsy-based diagnoses having revealed 13 benign and 8 malignant lesions ($p = 0.1161$). Focusing on positive confirmation or

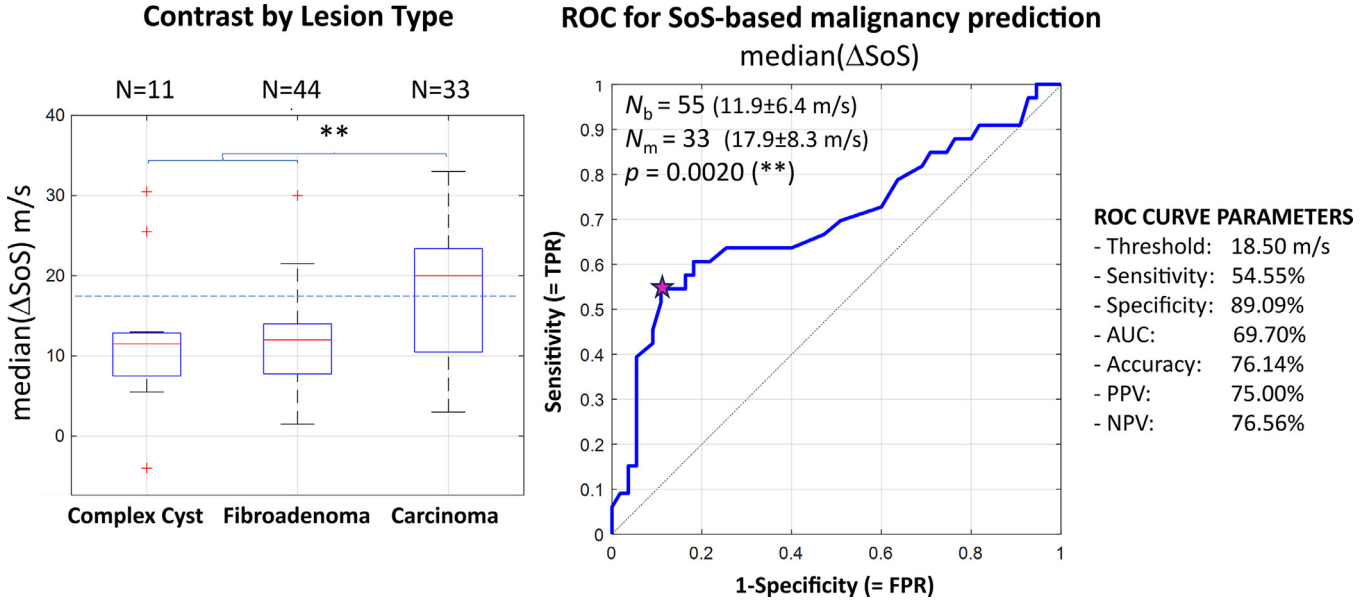

Figure 3. Box plot diagram and receiver operator characteristic (ROC) curves for speed of sound (SoS)-based malignancy prediction between benign (complex cysts and fibroadenoma, excluding simple cysts) and malignant (invasive carcinoma) lesions for all patients. Group sizes, statistical significance, key operating points (SoS contrast threshold as a dashed line in the box plot diagram and * on the ROC curve) and corresponding performance metrics are displayed.

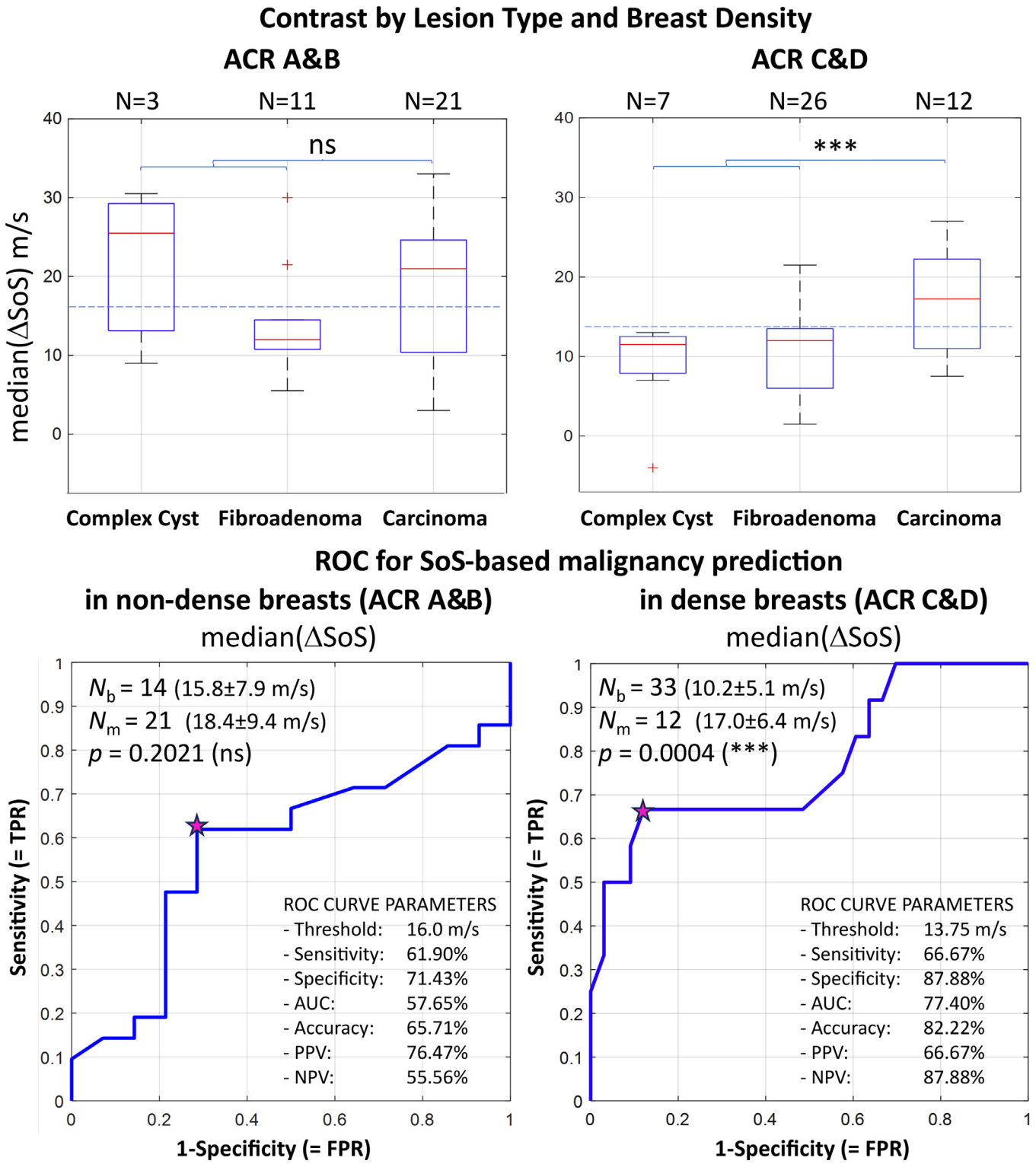

Figure 4. Box plot diagram and receiver operator characteristic curves for speed of sound-based malignancy prediction between benign and malignant lesions for patients with non-dense breasts (American College of Radiology [ACR] [a and b], *left column*) and for dense breasts (ACR [c and d], *right column*). Statistical significance, key operating points and corresponding performance metrics are displayed.

negative exclusion of malignancy with high probability, we considered two separate thresholds, where the lesions above an upper threshold could be considered to be malignant while those below a lower threshold as being benign. With a threshold of 30.25 m/s, a specificity and a PPV of 100% were achieved, with an overall accuracy of 71.41% (95% CI: 47.6%–90.5%). Alternatively, a threshold of 4.50 m/s achieved 100% sensitivity and NPV, with an overall accuracy of 52.38% (95% CI: 28.6%–71.4%). With those two thresholds we could identify three benign and one malignant out of 21 (19%) BI-RADS 4 lesions.

Discussion

The results confirm the technical and practical feasibility of speckle shift-based SoS imaging of breast lesions using pulse-echo US techniques

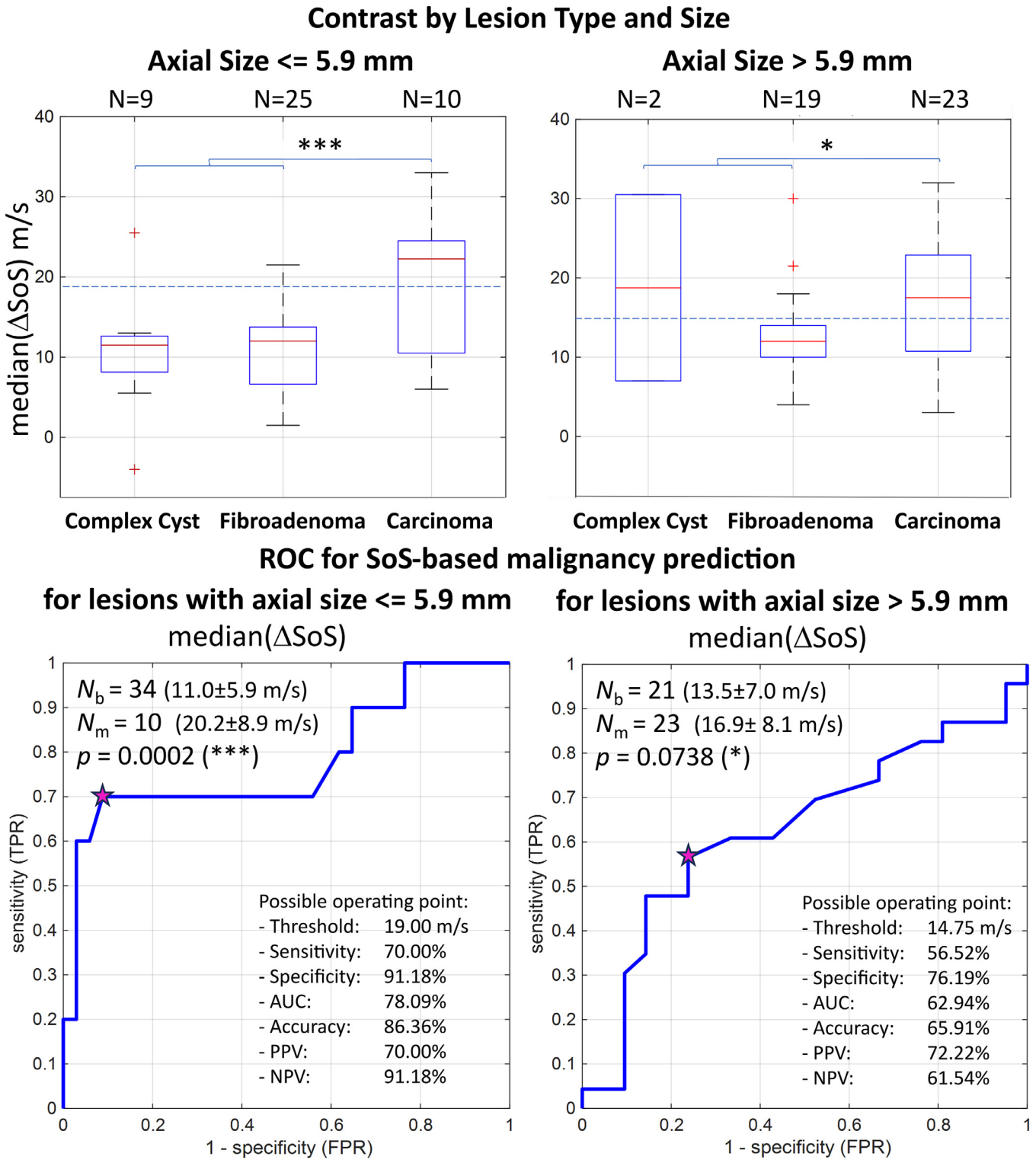

Figure 5. Box plot diagram and receiver operator characteristics curves for speed of sound-based malignancy prediction between benign and malignant lesions, stratified by axial lesion size: (*left column*) less than or equal to 5.9 mm, and (*right column*) greater than 5.9 mm. Statistical significance, key operating points and corresponding performance metrics are displayed.

with a handheld transducer. The measured absolute SoS inside the different lesion types (1464–1599 m/s) aligns with the findings of 1460–1560 m/s reported by Li et al. [8] using through-transmit acquisitions, but were achieved here with a much simpler hardware setup. This tested SoS imaging method shows promise as a novel imaging biomarker for tissue characterization.

When all lesions are considered as shown in Figure 3, the utilized malignancy prediction pipeline achieved high specificity, although the sensitivity remained relatively lower. For the subset of BI-RADS 4 lesions (Fig. 6), where the ability to predict or exclude malignancy based on conventional BUS exam was limited, the evaluated approach offered an SoS contrast threshold set to narrow down the candidates for biopsy

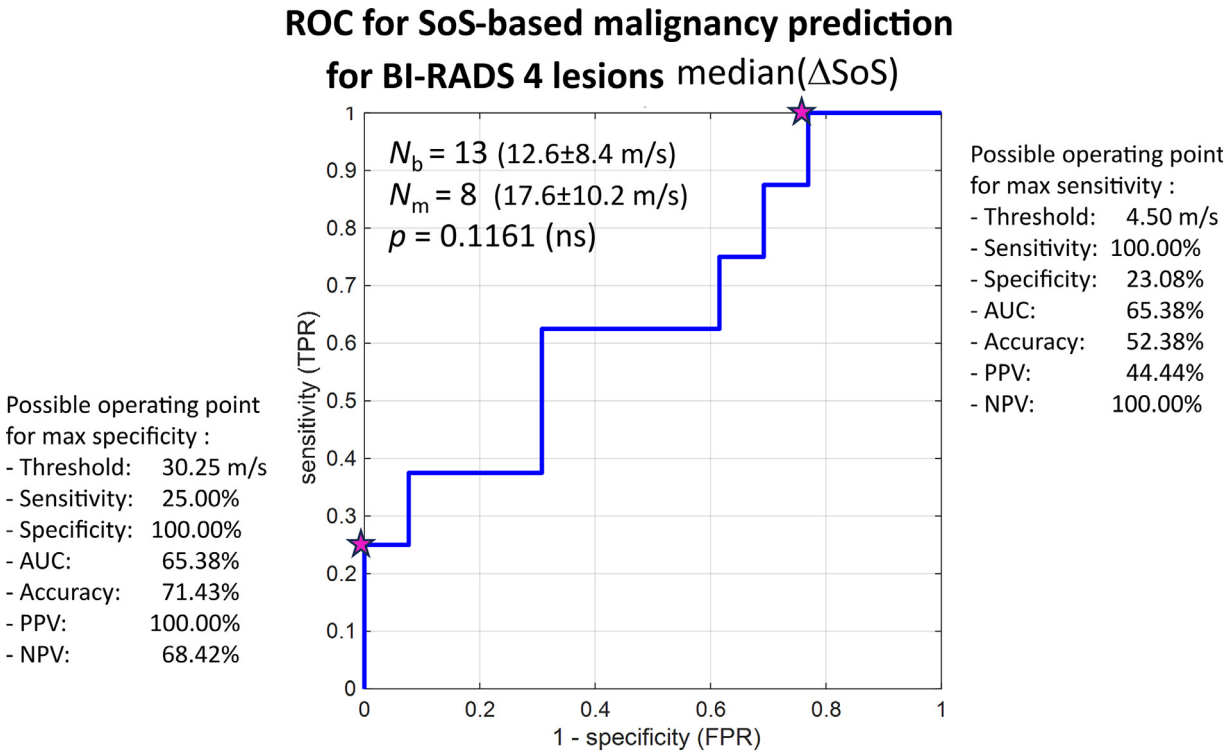

Figure 6. Receiver operator characteristic curves for speed of sound-based prediction of malignancy of BI-RADS 4 lesions between benign (complex cysts and fibroadenoma, excluding simple cysts) and malignant (invasive carcinoma). Key operating points, showing high specificity (30.25 m/s) and high sensitivity (4.50 m/s), along with their corresponding performance metrics are highlighted.

exam. A stratified analysis by breast density (Fig. 4, right column) demonstrated improved accuracy, in particular higher specificity, for patients with dense breasts. Additionally, as seen in Figure 5, our results indicate that SoS contrast was more indicative of cancer classification for smaller lesions, which could be due to the intrinsics of the reconstruction algorithm having access to displacements around and below a smaller inclusion or due to some pathological characteristic of smaller lesions.

From a clinical point of view, identifying truly benign lesions is as important as the identification of malignant ones and improves the assessment, especially for BI-RADS 3 findings, by potentially reducing unnecessary follow-ups and emotional stress for patients. By integrating SoS into routine BUS, diagnostic confidence can be improved and patient management optimized.

Malignant breast tumors are known to exhibit higher SoS values than their surrounding tissue [4,5]. Accordingly, to predict malignancy in this study, we explored the use of SoS contrast of lesions relative to their surrounding tissue, thereby compensating for variations in overall breast SoS, *e.g.*, by age [26] or menstrual cycle [27]. The evaluation of actual SoS values of lesions (or surroundings) *in vivo* would require mechanical testing of excised tissue samples, which was not available in this study and, although informative, presents its own challenges and limitations.

Our findings confirm that including SoS imaging into BUS exams could provide valuable complementary information for breast cancer differential diagnosis. Although higher lesion differentiation accuracy was reported by Ruby et al. [23], this was considering the maximum value in either the entire US view or a much larger area than the lesions themselves; hence, potentially not easily generalizable and applicable. Furthermore, only a small patient set was considered, with fibroadenomas being the only benign lesion type. Our assessment metric in this work only considered the lesion area as delineated by the radiologist, used a 95%-ile as a CI for robustness to sporadic SoS pixels, used an unambiguous definition of breast tissue background and assessment metric, facilitated multiple frames, assessed various lesion types, and studied a large patient set—all providing a more comprehensive evaluation for closely reflecting real-life clinical utility. This is the first time that motion-robust VS sequence has been studied in a patient cohort, which helped us to achieve highly improved lesion localization and contrast within the images. Future potential improvements of SoS data acquisition, pre-processing, and tomographic reconstruction pipelines, such as using learned imaging models [28], are envisioned to further enhance the reported results.

Although B-mode images may not always be indicative for cancer differential diagnosis, lesions are typically visible in B-mode. By choosing a maximum-like (95%-ile) SoS value inside the delineated inclusion, we aimed to minimize predicted SoS contrast sensitivity to potentially observer-dependent variations in lesion border delineations. Furthermore, we ensured statistical robustness by combining multiple SoS contrast measurements for each inclusion using the median operator, assuming that all measurements were equally reliable. In future studies, multiple annotators could be employed to check for possible SoS and contrast sensitivity to inter-annotator variation.

However, operator motion [24] or other factors may corrupt some readings. In future, one may consider incorporating measurement reliability during joint lesion prediction. The deeper regions in the reconstructions (*e.g.*, beyond <3 cm in Fig. 1 and 2) lack tissue SoS details and tend toward the background SoS due to the lack of further-below displacement measurements as input to reconstruct those image values. Few such deep measurements are often excluded from reconstruction due to their typical noise failing the quality threshold in tracking. Such a lack of SoS detail is, nevertheless, not anticipated to affect the utilized SoS contrast metric, as these deeper SoS values are part of the considered background, and furthermore the median is employed for robustness. Future studies should evaluate which tissue and reconstruction regions can best represent the breast background, *e.g.*, by manually excluding deeper locations or annotating a well-defined non-tumor breast area as the reference background.

Conclusion

In this study, raw US data were collected from various types of benign and malignant breast lesions and processed for SoS contrast measurements, demonstrating the feasibility of *in vivo* measurement of such quantitative US biomarkers based on speckle shifts using pulse-echo methods in a clinical setup. When combined with additional factors such as breast density and lesion size, SoS has been observed to be a valuable imaging biomarker that can contribute to the differential diagnosis of breast lesions. Despite the given moderate sample sizes, especially for the stratified sub-analyses, this study hopes to serve as a stepping stone in SoS imaging of the breast. Further advancements toward real-time SoS acquisition and processing capabilities are needed to enable instantaneous feedback during US examinations, either as an image overlay or as a quantitative SoS value within an operator-specified region or marker. Such enhancements could also include improvements in SoS image-reconstruction techniques to strengthen its ability to effectively classify lesions.

Conflict of interest

The authors declare no conflict of interest.

Acknowledgments

Research funding was provided by the Swiss National Science Foundation. Additional funding for the administration of clinical studies was provided by Bayer Schweiz AG and BRACCO Suisse SA, with partial support from the Young Researchers Grant of the European Society of Breast Imaging. The authors also appreciate the kind donation by the International School of Geneva with their Pink Day proceeds. Study monitoring was conducted by the digital Trial Intervention Platform (dTIP) at ETH Zurich, and statistical analysis was planned in collaboration with NEXUS Personalized Health Technologies at ETH Zurich. The authors also thank the staff at Kantonsspital Baden, particularly the study nurse Silke Callies, for their generous help and support.

Data availability statement

The ethics permission and patient consents do not allow the redistribution of the data.

References

[1] Mendelson EB, Böhm-Vélez M, Berg WA, et al. ACR BI-RADS Ultrasound. ACR BI-RADS Atlas, Breast Imaging Reporting and Data System. Reston, Virginia: American College of Radiology; 2013. p. 128–31.
[2] Barr RG, Nakashima K, Amy D, Cosgrove D, Farrokh A, Schafer F, et al. WFUMB guidelines and recommendations for clinical use of ultrasound elastography: Part 2: breast. Ultrasound Med Biol 2015;41:1148–60.
[3] Glozman T, Azhari H. A method for characterization of tissue elastic properties combining ultrasonic computed tomography with elastography. J Ultras Med 2010; 29:387–98.
[4] Bamber JC, Hill CR. Ultrasonic attenuation and propagation speed in mammalian tissues as a function of temperature. Ultras Med Biol 1979;5:149–57.
[5] Goss S, Johnston R, Dunn F. Comprehensive compilation of empirical ultrasonic properties of mammalian tissues. J Acoust Soc Am 1978;64:423–57.
[6] Pratt RG, Huang L, Duric N, Littrup P. Sound-speed and attenuation imaging of breast tissue using waveform tomography of transmission ultrasound data. SPIE Med Imaging Phys Med Imaging 2007;6510:65104S.
[7] Duric N, Littrup P, Poulo L, Babkin A, Pevzner R, Holsapple E, et al. Detection of breast cancer with ultrasound tomography: first results with the computed ultrasound risk evaluation (CURE) prototype. Med Phys 2007;34:773–85.
[8] Li C, Duric N, Littrup P, Huang L. *In vivo* breast sound-speed imaging with ultrasound tomography. Ultrasound Med Biol 2009;35:1615–28.
[9] Gemmeke H, Ruiter NV. 3D ultrasound computer tomography for medical imaging. Nucl Instrum Methods Phys Res 2007;580:1057–65.
[10] Malik B, Terry R, Wiskin J, Lenox M. Quantitative transmission ultrasound tomography: imaging and performance characteristics. Med Phys 2018;45:3063–75.
[11] Sanabria SJ, Goksel O. Hand-held sound-speed imaging based on ultrasound reflector delineation. MICCAI; 2016. p. 568–76.
[12] Rau R, Unal O, Schweizer D, Vishnevskiy V, Goksel O. Frequency-dependent attenuation reconstruction with an acoustic reflector. Med Image Anal 2021;67:101875.
[13] Jaeger M, Held G, Peeters S, Preisser S, Grunig M, Frenz M. Computed ultrasound tomography in echo mode for imaging speed of sound using pulse-echo sonography: proof of principle. Ultrasound Med Biol 2015;41:235–50.
[14] Sanabria SJ, Ozkan E, Rominger M, Goksel O. Spatial domain reconstruction for imaging speed-of-sound with pulse-echo ultrasound: simulation and in vivo study. Phys Med Biol 2018;63.
[15] Stahli P, Kuriakose M, Frenz M, Jaeger M. Improved forward model for quantitative pulse-echo speed-of-sound imaging. Ultrasonics 2020;108:106168.
[16] Rau R, Schweizer D, Vishnevskiy V, Goksel O. Speed-of-sound imaging using diverging waves. Int J Comput Assist Radiol Surg 2021;16:1201–11.
[17] Anderson ME, Trahey GE. The direct estimation of sound speed using pulse-echo ultrasound. J Acoust Soc Am 1998;104:3099–106.
[18] Jakovljevic M, Hsieh S, Ali R, Chau Loo Kung G, Hyun D, Dahl JJ. Local speed of sound estimation in tissue using pulse-echo ultrasound: model-based approach. J Acoust Soc Am 2018;144:254–66.
[19] Imbault M, Faccinetto A, Osmanski BF, Tissier A, Deffieux T, Gennisson JL, et al. Robust sound speed estimation for ultrasound-based hepatic steatosis assessment. Phys Med Biol 2017;62:3582.
[20] Bendjador H, Deffieux T, Tanter M. Novel approach for ultrafast aberration correction and real-time speed-of-sound mapping. In: Byram BC, Ruiter NV, editors. Med Imaging Ultrason Imaging Tomogr. SPIE; 2021:116020B.
[21] Heriard-Dubreuil B, Besson A, Wintzenrieth F, Cohen-Bacrie C, Thiran JP. Refraction-based speed of sound estimation in layered media: an angular approach. IEEE Trans Ultrason Ferroelectr Freq Control 2023;70:486–97.
[22] Wang X, Bamber JC, Esquivel-Sirvent R, Ormachea J, Sidhu PS, Thomenius KE, et al. Ultrasonic sound speed estimation for liver fat quantification: a review by the AIUM-RSNA QIBA pulse-echo quantitative ultrasound initiative. Ultrasound Med Biol 2023;49:2327–35.
[23] Ruby L, Sanabria SJ, Martini K, Dedes KJ, Vorburger D, Oezkan E, et al. Breast cancer assessment with pulse-echo speed of sound ultrasound from intrinsic tissue reflections: proof-of-concept. Invest Radiol 2019;54:419–27.
[24] Schweizer D, Rau R, Bezek CD, Kubik-Huch RA, Goksel O. Robust imaging of speed of sound using virtual source transmission. IEEE Trans Ultrason Ferroelectr Freq Control 2023;70:1308–18.
[25] Aleskandarany MA, Vandenberghe ME, Marchio C, Ellis IO, Sapino A, Rakha EA. Tumour heterogeneity of breast cancer: from morphology to personalised medicine. Pathobiology 2018;85:23–34.
[26] Bezek CD, Farkas M, Schweizer D, Kubik-Huch RA, Goksel O. Breast density assessment via quantitative sound-speed measurement using conventional ultrasound transducers. Eur Radiol 2025;35:1490–501.
[27] Ruby L, Sanabria SJ, Obrist AS, Martini K, Forte S, Goksel O, et al. Breast density assessment in young women with handheld ultrasound based on speed of sound: influence of the menstrual cycle. Medicine 2019;98:e16123.
[28] Bezek CD, Haas M, Rau R, Goksel O. Learning the imaging model of speed-of-sound reconstruction via a convolutional formulation. IEEE Trans Med Imaging 2024:PP (99). doi: 10.1109/TMI.2024.3480690.